EXPLORING HALF-METALLIC FERROMAGNETISM IN II-IV-V_2 CHALCOPYRITE'S FOR SPINTRONIC APPLICATIONS

Abstract

This research investigates new magnetic materials (II-IV-V_2 chalcopyrite's) for spintronic applications. Using first-principles calculations with density functional theory (DFT), the study explores their structural, electronic, and magnetic properties. The compounds exhibit stable ordered body-centered tetragonal (BCT) chalcopyrite structures, with some displaying half-metallic ferromagnetic behavior. $ZnMX_2$ and $CdMX_2$ (M = V, Cr, Mn; X = P, As) compounds exhibit strong half metallic (HM) property, while $ZnFeX_2$ and $CdFeX_2$ show stable ferromagnetic (FM) property. Theoretical predictions suggest that the $ZnMX_2$ and $CdMX_2$ (M = V, Cr, Mn) are potential spin injectors for spintronic devices. This work highlights the significance of LSDA and GGA exchange-correlation effects in determining the materials half-metallicity, structural stability, and ground-state properties. Perhaps, the present study provide valuable insights for further experimental investigations and materials design in spintronics.

Keywords: Half-metallic ferromagnetism, Chalcopyrite's, Spintronic materials, Density functional theory, electronic band structure

Authors

D Vijayalakshmi
Department of Physics
Vels Institute of Science
Technology & Advanced Studies (VISTAS)
Chennai, Tamil Nadu, India

G Jaiganesh
Excel Instruments
Dias Industrial Estate
Vasai East, Sativali Naka, India

R Umamaheswari
Department of Physics
College of Engineering
Anna University
Chennai, Tamil Nadu, India.

G Kalpana
Department of Physics
Vels Institute of Science
Technology & Advanced Studies (VISTAS)
Chennai, Tamil Nadu, India

I. INTRODUCTION

First-principal calculations, or ab-initio calculations, provide a realistic understanding of electrons in solids based on quantum mechanics, statistical thermodynamics, classical mechanics, and electrodynamics [1]. Researchers use computer-based modeling, integrating theories and algorithms from various disciplines, to unravel the physical and chemical properties of materials, offering valuable insights not easily obtained through experiments alone. These simulations enable predictions of solid behaviors under extreme conditions, facilitating diverse applications [1]. The study of electron behavior, including mass, charge, and spin, has led to a transformative era in microelectronics, giving rise to spintronics - a groundbreaking field integrating spin and charge for electronic devices. Spintronics promises solutions to electronic challenges and has rapidly grown under the term 'magneto-electronics' [2]. Spintronic random access memory (RAM) chips offer higher storage density and faster switching, demanding compact and robust dimensions. Highly spin-polarized materials enable efficient spin injection, leading to significant magnetoresistance effects in devices like spin filters, spin diodes, and spin field-effect transistors (FETs) [2]. Researchers focus on novel spintronic materials, optimizing spin-polarized transport, investigating spin relaxation, and developing spin-injection techniques, driving advancements in electronic devices and spintronics applications.

The exploration of transition metal (TM) ion-doped ternary semiconductors has garnered significant attention due to experimental confirmations of high Curie temperatures (T_C) in chalcopyrite compounds [3,4] . The occurrence of ferromagnetic (FM) or antiferromagnetic (AFM) characteristics depends on the substitutional site of TM atoms, whether at the cationic site Zn or Si. Notably, Rufinus [5] conducted first-principal calculations on M-doped (M = Mn, Cr, or V) ternary material $ZnSiN_2$ to investigate whether substitutional TM atoms at the group II (Zn) site and group IV (Si) site exhibit FM or AFM behavior. The study revealed intriguing FM behavior when V was doped at both the Zn and Si cation sites of $ZnSiN_2$.

In this manuscript, our focus revolves around the investigation of chalcopyrite materials. Specifically, we delve into two categories: the I-III-VI_2 and II-IV-V_2 type compounds, which are commonly known as chalcopyrite-structured compounds. These compounds have their origins traced back to the chalcopyrite mineral $CuFeS_2$, giving rise to various possibilities through combinations of I-III-VI_2 and II-IV-V_2 elements. The synthesis and structural characterization of I-III-VI_2 chalcopyrite's were first undertaken by Hahn et al. in 1953, and Goodman and Douglas [6] later discussed their potential for semi-conductivity. Chalcopyrite semiconductors, composed of non-toxic elements, have proven to possess a suitable band gap and absorption coefficient greater than conventional direct band gap semiconductors, rendering them inexpensive and highly attractive for a wide array of applications.

Our literature review encompasses various investigations related to the substitution of group IV atoms in sulphur and selenium-based copper gallium chalcopyrite $CuGaX_2$ (X = S and Se). These materials exhibit tremendous potential for both photovoltaic and spintronic applications. Additionally, research on Mn-doped $CdGeP_2$ revealed half-metallic ferromagnetism (HMF) [7]. Furthermore, experimental results on $Zn_{1-x}Mn_xGeP_2$ displayed stable AFM behavior and p-type characteristics at specific temperatures [8]. First-principal

calculations by Picozzi et al. [9] on Mn-doped $CuGaS_2$ demonstrated the favouritism for FM behavior via carrier-mediated interaction. Studies by Yu & Yao [10] explored the HMF properties in chalcopyrite $ZnCrAs_2$. Furthermore, researchers have investigated Mn-doped $ZnSnAs_2$ epilayers and analyzed the relationship between Mn concentration and T_C in $(Zn,Mn,Sn)As_2$ [11, 12].

Bulk II-IV-V_2 chalcopyrite crystals have been synthesized experimentally, and researchers have made strides in engineering materials at the nanoscale to achieve fascinating and unconventional physical properties. The quest for optimized nanomaterials that transport and generate spin-polarized carriers in spintronics represents a burgeoning field of research. These endeavours enable predictions and provide a deeper understanding of the magnetic properties of chalcopyrite semiconductors.

Motivated by the discussions and literature on $ZnCrAs_2$ [13] and $CuCrSe_2$, [14] as well as the experimental synthesis on $ZnSnAs_2$:Mn, $MnGeAs_2$, and $MnGeP_2$ chalcopyrite materials, the present study aims to provide fresh predictions on new chalcopyrite semiconductors. In the present study, the electronic, magnetic, and ground state properties of $ZnMX_2$ and $CdMX_2$ are studied within different exchange and correlation potential, such as generalized gradient approximation (GGA) and local spin density approximation (LSDA), using full potential - linearized augmented plane wave (FP-LAPW) method as implemented in the WIEN2k code. The effect of substitution of M (Sc, Ti, V, Cr, Mn, Fe; X = P, As; Y = S, Se) atoms in the Ge site of $ZnGeP_2$, $ZnGeAs_2$, $CdGeP_2$, $CdGeAs_2$ chalcopyrite's and their results are compared with available reported values.

Crystal Structure: The chalcopyrite structure is obtained by doubling the zinc blende (ZB) structure along the c-axis, resulting in a tetragonal unit cell (Figure 1. a). Its chemical formula is II-IV-V_2 (II = Zn, Cd; IV = Ge; V = P, As). The doubled structure leads to each V anion being coordinated by two II and two IV cations, and each cation being tetrahedrally coordinated by four anions, creating a body-centred tetragonal (BCT) Bravais lattice. Consequently, the chalcopyrite structure's primitive cell contains eight atoms compared to the ZB structure's primitive cell with two atoms (Figure 1.b).

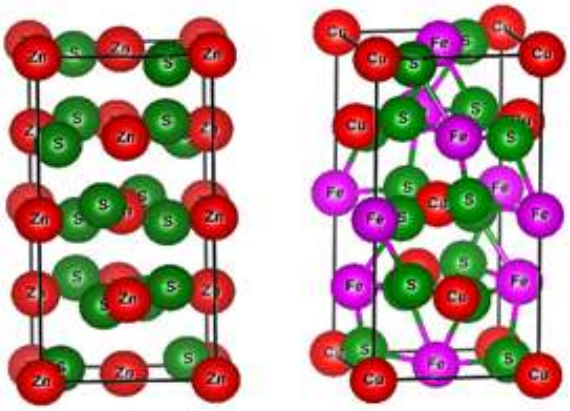

Figure 1: (a) Crystal Structure of Zinc-Blende Unit Cell Doubled Along the Crystal C Axis (b) Chalcopyrite $CuFeS_2$

The molecular formula for the chalcopyrite structure is is II-IV-V_2 (II = Zn, Cd; IV = Ge; V = P, As). The atomic positions in the chalcopyrite structure are given as follows: II (0, 0, 0), (0, 1/2, 1/2); IV(1/2, 1/2, 0); (1/2, 0, 1/4), V(*u*, 1/4, 1/8); (*u*, 3/4, 1/8); (3/4, *u*, 7/8); (1/4, *u*, 7/8), where u represents the anion displacement. This distortion along the crystal c-axis causes the tetrahedron to be irregular, deviating the *c/a* ratio from the ideal value of 2.0 (Figure 1.b). The internal parameter (*u*), lattice positions (a_o, c_o), and their corresponding bond lengths in Å are listed in Table 1 for the chalcopyrite hosts used in this study.

Table 1: Internal Parameter (*u*), Lattice Constants (a_o , c_o), and Bond Length in Å Respectively of Chalcopyrites Hosts Used In This Manuscript

Compounds	Internal parameter *(u)*	Lattice constant (Å)		Bond length (Å)		References
		a_o	c_o	A-B	B-C	
$ZnGeP_2$	0.250[a], 0.254[b] 0.258[c]	5.41[a], 5.50[b]	10.60[a], 10.85b,			15
$ZnGeAs_2$	0.249[a], 0.267[b]	5.63[a], 5.66[b]	0.988[a], 11.15[b]			16, 17
$CdGeP_2$	0.279[a], 0.283[b]	5.66[a], [b]	11.22[a], [b]			18, 19
$CdGeAs_2$	0.265[a], 0.278[b]	5.91[a], 5.94[b]	11.91[a], 11.21[b]	2.57[a] 2.58[b]	2.47[a] 2.47[b]	20, 21
$CuGaS_2$	0.249[a]	5.37[a]	10.74[a]			22
$CuGaSe_2$	0.243[a], 0.244[b]	5.67[a], 5.67[b]	11.63[a], 11.34[b]			7, 8, 10, 13
$AgGaS_2$	0.284[a], 0.282[b]	5.77[a],	11.54[a],			16, 20
$AgGaSe_2$	0.250[a], 0.279[b] 0.272[c]	5.99[a], 6.05[b]	11.19[a] ,12.08[b]			16, 21 20

II. COMPUTATIONAL METHODOLOGY

The structural, electronic and magnetic properties of ternary $ZnMX_2$ and CdMX2 (M = Sc, Ti, V, Cr, Mn, Fe; X = P, As) compounds in the BCT chalcopyrite structure have been carried out using FP-LAPW method [23] as implemented in WIEN2k package [24]. GGA proposed by Perdew-Berke-Ernzerhof (PBE) [25] and LSDA given by J.P. Perdew and Y. Wangis [26] are used for the exchange correlation potential. For the self-consistent calculations, the unit cell is divided into two regions, namely, non-overlapping atomic sphere and interstitial regions.

A linear combination of spherical harmonic functions up to l_{max} = 12 is used in the atomic sphere region and a plane wave cutoff value was set at K_{max} = 8.0 Ryd in the interstitial region. The electrons in the atomic sphere region are core electrons which are treated fully relativistic and valence electrons in the interstitial region are considered semirelativistically. The muffin–tin radii (RMT) for Zn, Ge, P, As, Sc, Ti, V, Cr, Mn and Fe are set to 2.23 a.u., 2.25 a.u., 2.16 a.u., 2.10 a.u., 2.22 a.u., 2.24 a.u., 2.27 a.u. 2.16 a.u., 2.18 a.u. and 2.25 a.u., respectively. Atomic sphere radii chosen are 2.08, 2.13, 2.12, 2.18, 2.23, 2.24, 2.17, 2.20 and 2.09 for Cd, Sc, Ti, V, Cr, Mn, Fe, P and As respectively. The charge density is Fourier expanded upto Gmax = 12. From the relaxed geometry, electronic

structure, electronic charge density and the magnetic properties can be determined. A k mesh of 8 x 8 x 4 for k-points integration in the irreducible wedge of the first Brillouin zone is used. Self-consistent total energy convergence of the crystal to a value of less than 0.01 mRy is achieved by the method of iteration.

III. RESULTS AND DISCUSSION

We present comprehensive *ab-initio* calculations of chalcopyrite Zn/$CdMX_2$ (M = Sc, Ti, V, Cr, Mn, Fe; X = P, As) compounds, investigating their structural and magnetic properties using the FP-LAPW method within GGA and LSDA. Our study includes the determination of internal parameters, tetragonal ratio, equilibrium lattice constants, bulk modulus, bond lengths, and heat of formation for non-magnetic (NM), ferromagnetic (FM), and antiferromagnetic (AFM) states of all $ZnMX_2$ compounds. Additionally, we explore the exhibition and stability of the FM state through spin-polarized and spin-unpolarized calculations. Furthermore, we extend our investigation to $CdMX_2$ compounds, introducing TM (Sc, Ti, V, Cr, Mn, Fe) impurities at the Ge site of $CdGeX_2$. The results reveal attractive electronic and magnetic properties in these chalcopyrite's, leading to the prediction of half-metallic ferromagnetism in $CdMX_2$ compounds for the first time.

1. **Structural Properties and Magnetism:** The total energy is fitted to Birch-Murnaghan's equation of state [27] to determine essential structural parameters (*u, c/a,* a_0*,* c_0*, and* B_0) for non-magnetic (NM), ferromagnetic (FM), and antiferromagnetic (AFM) states in the body-centred tetragonal (BCT) chalcopyrite structure of $ZnMX_2$ (M = Sc, Ti, V, Cr, Mn, Fe; X = P, As) compounds in Table 2 and 3. The minimum energy of $ZnMX_2$ (V, Cr, Mn, Fe) compounds is found in the FM state (Fig. 2), indicating induced magnetism upon incorporating M (V, Cr, Mn, Fe) atoms in the NM $ZnGeP_2$/As_2. Negative energy differences (ΔE_1 and ΔE_2) for $ZnMX_2$ (M = V, Cr, Mn, Fe) confirm their FM stability, while $ZnScX_2$ and $ZnTiX_2$ remain stable in the NM state. Calculated negative formation energy (*ΔH*) further supports the stability of these compounds for experimental synthesis.

   Ground state properties of $CdMX_2$ (M = Sc, Ti, V, Cr, Mn, Fe; X = P, As) compounds in the chalcopyrite structure are investigated using total energy-volume relations for NM, FM, and AFM states. The stability of the magnetic state is estimated from spin-polarized energy differences (ΔE_1 and ΔE_2). $CdScX_2$ and $CdTiX_2$ exhibit ΔE_1 and ΔE_2 values are zero, indicating NM state at equilibrium. Conversely, negative ΔE_1 and ΔE_2 values for $CdMX_2$ (M = V, Cr, Mn, Fe) in Table 4 and 5 suggest FM state is more favourable in these compounds. Additionally, negative formation energy (*ΔH*) confirms the energetic preference of these compounds when M atoms occupy the group IV (Ge) position in $CdGeX_2$. Similar observations are found for both the $ZnMX_2$ and $CdMX_2$ in this manuscript we are presenting the figures for $ZnMX_2$ compounds using GGA. Figure 2 displays the total energy-volume curve for all the $ZnMX_2$ compounds. $CdMX_2$ in this manuscript we are presenting the figures for $ZnMX_2$ compounds using GGA. Figure 2 displays the total energy-volume curve for all the $ZnMX_2$ compounds.

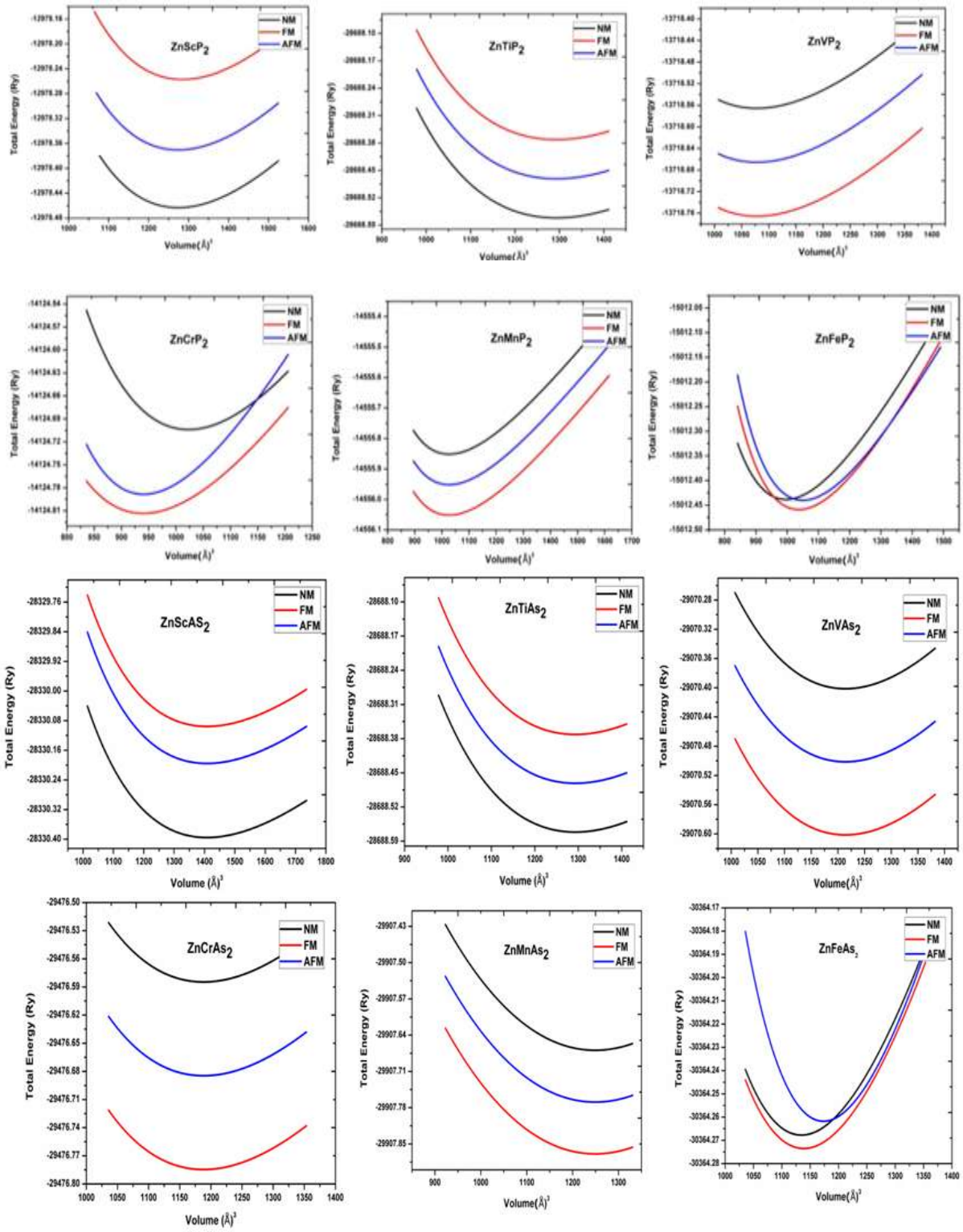

Figure 2: Total Energy (Ry) / f.u. as a Function of Volume ($Å^3$) Plots for Body-Centered Tetragonal (BCT) Chalcopyrite Structures of $ZnMX_2$ (M = Sc, Ti, V, Cr, Mn, Fe; X = P, As) Compounds

Table 2: Calculated Intern al Parameter (u), Equilibrium Lattice Constants (a_0, c_0) in Å, and Bulk Modulus (B_0) in GPa for Nonmagnetic (NM), Ferromagnetic (FM) and Antiferromagnetic (AFM) Phases of Body Centred Tetragonal (BCT) Chalcopyrite Type $ZnMX_2$ (M = Sc, Ti, V, Cr, Mn, Fe; X = P, As), Total Energy Difference ΔE_1 ($\Delta E_1 = E_{FM}-E_{NM}$) in meV/cell, ΔE_2 ($\Delta E_2 = E_{FM}-E_{AFM}$) in meV/cell using GGA

Compounds	NM				FM				AFM				ΔE_1	ΔE_2
	u	a_0	c_0	B_0	u	a_0	c_0	B_0	u	a_0	c_0	B_0		
$ZnGeP_2$	0.262	5.41	10.68	97.43	0.72	5.38	10.56	91.56	0.283	0.267	5.46	10.70	-	-
Other	0.267[a]	5.46[a]	10.70[a]	98.12	-	-	-	-	-	-	-	-	-	-
$ZnScP_2$	0.242	5.41	10.71	96.13	0.24	5.46	10.76	93.31	0.257	5.40	10.71	93.01		
$ZnTiP_2$	0.253	5.40	10.67	90.63	0.26	5.44	10.72	89.03	0.270	5.42	10.78	89.83	-	-
$ZnVP_2$	0.241	5.39	10.49	100.0	0.28	5.35	10.54	99.07	0.289	5.31	10.59	99.77	-2.12	-4.24
$ZnCrP_2$	0.262	5.28	10.30	157.0	0.21	5.26	10.36	156.03	0.220	5.20	10.37	156.93	-7.13	-7.46
$ZnMnP_2$	0.270	5.26	10.27	110.0	0.22	5.23	10.30	109.23	0.221	5.19	10.36	109.63	-5.23	-4.89
$ZnFeP_2$	0.290	5.88	11.49	109.0	0.24	5.85	11.51	105.87	0.242	5.82	11.57	106.07	-4.56	-5.79
$ZnGeAs_2$	0.263	5.48	10.89	78.6	0.26	5.66	11.15	88.05	0.264	5.66	11.15	76.35		
Other	0.264[a]	5.66[a]	11.15[a]	-	-	-	-	-	-	-	-	-	-	-
$ZnScAs_2$	0.249	5.69	11.00	75.08	0.24	5.66	11.13	73.98	0.250	5.63	11.17	74.08		
$ZnTiAs_2$	0.250	5.68	11.02	77.04	0.26	5.65	11.12	75.64	0.271	5.62	11.14	75.94	-	-
$ZnVAs_2$	0.268	5.52	10.72	79.72	0.27	5.48	10.78	78.02	0.279	5.44	10.79	78.72	-2.32	-2.06
$ZnCrAs_2$	0.298	5.59	10.89	92.98	0.21	5.56	10.94	90.78	0.217	5.51	10.99	90.98	-7.06	-6.10
$ZnMnAs_2$	0.208	5.56	10.79	89.18	0.22	5.50	10.83	86.08	0.226	5.48	10.89	86.88	-5.68	-5.08
$ZnFeAs_2$	0.217	5.59	10.91	70.03	0.220	5.57	10.98	68.08	0.224	5.51	10.91	68.98	-3.24	-3.05

[a]Shay & Wernick (1975), **T**

Table 3: Calculated Heat of Formation (ΔH) in eV and Bond Length in Å of $ZnMX_2$ (M = Sc, Ti, V, Cr, Mn, Fe; X = P, As)

Compounds	NM			FM			AFM		
	ΔH	Bond length		ΔH	Bond length		ΔH	Bond length	
		Zn-Y	M-Y		Zn-Y	M-Y		Zn-Y	M-Y
$ZnGeP_2$	-27.7	2.34	2.34	-28.1	2.27	2.27	-27.8	2.21	2.21
$ZnScP_2$	-28.1	2.41	2.41	-28.6	2.52	2.52	-28.8	2.53	2.53
$ZnTiP_2$	-29.4	2.47	2.47	-29.6	2.44	2.44	-29.1	2.45	2.45
$ZnVP_2$	-27.9	2.45	2.35	-28.1	2.29	2.15	-28.8	2.24	2.54
$ZnCrP_2$	-28.3	2.34	2.24	-28.7	2.27	2.14	-28.1	2.21	2.13
$ZnMnP_2$	-23.9	2.53	2.43	-23.3	2.15	2.03	-23.7	2.13	2.08
$ZnFeP_2$	-35.9	2.48	2.68	-35.5	2.10	2.28	-35.9	2.11	2.01
$ZnGeAs_2$	-43.6	2.48	2.48	-43.3	2.28	2.28	-43.2	2.32	2.32
$ZnScAs_2$	-33.9	2.68	2.68	-33.1	2.48	2.48	-33.9	2.61	2.61
$ZnTiAs_2$	-42.8	2.53	2.53	-42.3	2.51	2.51	-42.5	2.53	2.53
$ZnVAs_2$	-47.6	2.55	2.65	-47.1	2.39	2.25	-47.7	2.32	2.28
$ZnCrAs_2$	-43.1	2.48	2.58	-43.2	2.18	2.08	-43.6	2.12	2.06
$ZnMnAs_2$	-45.6	2.66	2.86	-15.9	2.31	2.26	-15.8	2.33	2.27
$ZnFeAs_2$	-49.8	2.57	2.77	-49.1	2.23	2.57	-49.1	2.23	2.61

Table 4: Calculated Internal Parameter *(u)*, Equilibrium Lattice Constants (a_0, c_0) in Å, and Bulk Modulus (B_0) in GPa, Total Energy Difference ΔE_1 ($\Delta E_1 = E_{FM}-E_{NM}$) in meV/cell, ΔE_2 ($\Delta E_2 = E_{FM}-E_{AFM}$) in meV/cell between the Nonmagnetic (NM), Ferromagnetic (FM) and Antiferromagnetic (AFM) States of $CdMX_2$ (M = Sc, Ti, V, Cr, Mn, Fe; X = P, As) using GGA

Compounds	NM				FM				AFM				ΔE_1	ΔE_2
	u	a_0	c_0	B_0	u	a_0	c_0	B_0	u	a_0	c_0	B_0		
$CdGeP_2$	0.279	6.326	11.88	79.04	0.279	6.32	11.88	79.04	0.279	6.32	11.88	79.04	-	-
Others	0.283[a]	5.740[a]	10.77[a]											
$CdScP_2$	0.260	6.09	11.44	80.07	0.255	6.07	11.46	54.03	0.255	6.07	11.46	57.56	-	-
$CdTiP_2$	0.276	5.89	11.02	67.42	0.276	5.88	11.04	66.79	0.276	5.88	11.04	68.54	-	-
$CdVP_2$	0.304	5.79	10.91	72.68	0.303	5.78	10.92	69.65	0.304	5.77	10.90	67.10	-7.4	-7.8
$CdCrP_2$	0.303	5.84	11.05	76.03	0.302	5.86	11.07	55.34	0.301	5.89	11.05	61.09	-1.3	-6.8
$CdMnP_2$	0.308	5.67	10.73	78.12	0.285	5.69	10.76	70.52	0.302	5.71	10.78	75.65	-9.6	-5.3
$CdFeP_2$	0.301	5.62	10.56	95.01	0.300	5.60	10.58	95.08	0.308	5.62	10.60	93.28	-8.6	-5.5
$CdGeAs_2$	0.280	6.12	11.31	65.37	0.280	6.12	11.31	59.56	0.280	6.12	11.31	59.04	-	-
Others	0.278[a]	5.94[a]	11.216[a]											
$CdScAs_2$	0.252	6.25	11.81	43.96	0.252	6.24	11.80	47.60	0.251	6.26	11.82	38.58	-	-
$CdTiAs_2$	0.285	6.09	11.49	58.14	0.278	6.07	11.47	58.84	0.285	6.09	11.49	57.31	-	-
$CdVAs_2$	0.305	6.02	11.32	63.10	0.304	6.00	11.34	80.20	0.250	6.03	11.32	56.05	-9.8	-7.4
$CdCrAs_2$	0.307	6.04	11.35	64.46	0.306	6.02	11.37	55.73	0.305	6.04	11.35	59.04	-2.66	-2.49
$CdMnAs_2$	0.304	5.93	11.18	69.50	0.303	5.91	11.16	66.66	0.301	5.93	11.18	63.78	-9.51	-1.87
$CdFeAs_2$	0.302	5.89	11.11	79.75	0.301	5.87	11.09	65.89	0.308	5.89	11.08	78.77	-5.63	-5.94

Table 5: Calculated Heat of Formation (Δ*H)* in eV and Bond Length in Å for $CdMX_2$ (M = Sc, Ti, V, Cr, Mn, Fe; X = P, As) compounds using GGA

Compounds	NM			FM			AFM		
	ΔH	Bond length		*ΔH*	Bond length		*ΔH*	Bond length	
		Cd-Y	M-Y		Cd-Y	M-Y		Cd-Y	M-Y
$CdGeP_2$	-29.74	2.65	2.65	-29.56	2.68	2.68	-30.71	2.66	2.66
$CdScP_2$	-30.1	2.45	2.44	-30.4	2.45	2.45	-31.08	2.45	2.45
$CdTiP_2$	-31.4	2.45	2.45	-31.5	2.45	2.45	-30.3	2.45	2.45
$CdVP_2$	-29.9	2.65	2.45	-29.7	2.45	2.25	-31.7	2.43	2.23
$CdCrP_2$	-30.3	2.34	2.24	-30.5	2.14	2.04	-29.6	2.12	2.02
$CdMnP_2$	-25.9	2.33	2.23	-25.7	2.13	2.03	-30.8	2.11	2.01
$CdFeP_2$	-37.9	2.48	2.48	-37.7	2.28	2.28	-25.4	2.24	2.24
$CdGeAs_2$	-43.87	2.53	2.53	-44.34	2.52	2.52	-48.76	2.52	2.52
$CdScAs_2$	-35.9	2.48	2.48	-35.7	2.48	2.48	-36.7	2.44	2.44
$CdTiAs_2$	-44.8	2.33	2.23	-44.6	2.33	2.23	-35.5	2.33	2.21
$CdVAs_2$	-49.6	2.35	2.25	-49.4	2.35	2.25	-44.7	2.33	2.23
$CdCrAs_2$	-45.1	2.28	218	-45.3	2.28	218	-49.6	2.24	2.12
$CdMnAs_2$	-17.6	2.46	2.36	-17.4	2.11	2.06	-45.5	2.18	2.04
$CdFeAs_2$	-51.8	2.37	2.47	-51.6	2.13	2.27	-17.6	2.11	2.25

2. **Overlap of -3d States Induces Ferromagnetism/halfmetallicity:** Substituting M atoms (Sc, Ti, V, Cr, Mn, Fe) at the Ge site of $ZnGeX_2$ (X = P, As) compounds causes overlap between -3d (t_{2g} and e_g) states of M and nearest neighbour -p states of X, resulting in the emergence of ferromagnetic (FM) properties in some compounds. Spin-polarized calculations reveal that $ZnScX_2$ and $ZnTiX_2$ exhibit no effective spin polarization of energy states near the Fermi level (E_F), indicating their non-magnetic (NM) ground state. In contrast, $ZnMX_2$ (M = V, Cr, Mn, Fe) compounds display spin-splitting of energy states around the Fermi level (E_F), confirming their FM nature. Whereas, HMF property is observed in $ZnMX_2$ (M = V, Cr, Mn; X = P, As) compounds, where the valence bands cross the E_F in the spin-up channel (metallic behavior) and form a band gap near the E_F in the spin-down channel (semiconducting nature) with 100% spin-polarization around the E_F Spin splitting of energy band structures for $ZnVX_2$ structures is shown in Figure 3, similar observations for $ZnCrX_2$ and $ZnMnX_2$ was achieved. However, $ZnFeX_2$ exhibits spin-splitting around the E_F but lacks half-metallicity.

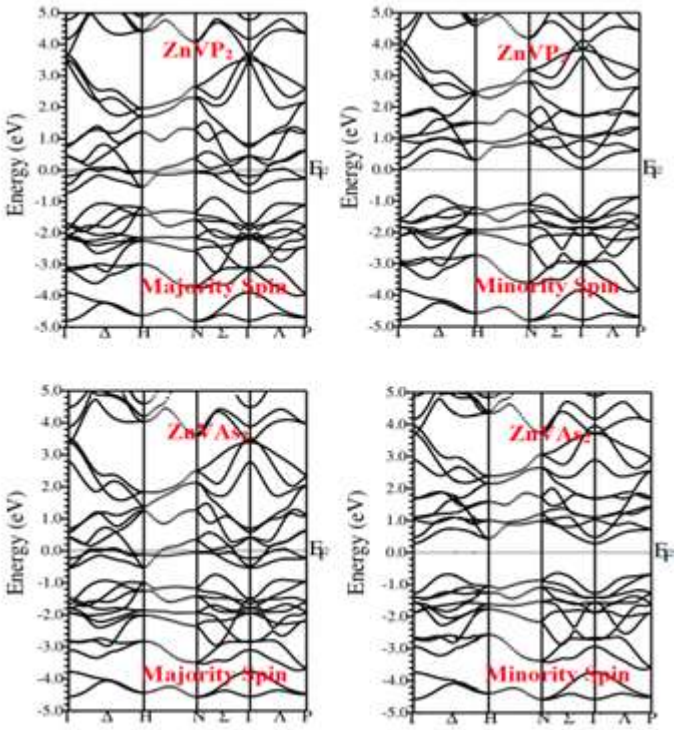

Figure 3: Spin Polarized Electronic Band Structures of $ZnVX_2$ (X = P, As)

$CdScX_2$ and $CdTiX_2$ demonstrate no spin polarization of energy states around the E_F, confirming their NM nature at equilibrium. Spin-polarized calculations for $CdMX_2$ (M = V, Cr, Mn, Fe; X = P, As) compounds exhibit spin-splitting of energy states near the E_F. $CdMX_2$ (M = V, Cr, Mn; X = P, As) compounds further display an energy gap around the E_F in the spin-down channel, while the spin-up channel exhibits metallic behavior, indicating the presence of HMF characteristics. HMF originates from the hybridization of partially filled *-3d(t_{2g})* states of M with nearest neighbour *-p* states of X (P, As) atoms, with minor contribution from Cd *s*-like states. $CdFeX_2$ shows stable FM with spin-splitting energy levels around the E_F, but lacks HMF at its equilibrium volume.

3. **Charge Densities:** To gain deeper insights into the origin of ferromagnetism and analyse the nature of chemical bonding and charge transfer in the compounds, two-dimensional (2D) charge spin density contour plots along the (110) plane are determined for the $ZnMX_2$ (M = Sc, Ti, V, Cr, Mn, Fe; X = P, As) compounds in both spin up and spin down states. These plots provide valuable information on the ionic and covalent characters of Zn-X and M-X atomic bonds.

The electron density plots for $ZnScX_2$ and $ZnTiX_2$ reveal that the charge density contours are spherical around X atoms, indicating a strong ionic bond with partial covalent bonding nature. However, in $ZnMX_2$ (M = V, Cr, Mn), the charge transfer between M and X ions results in a strong overlap due to effective hybridization of -3d states of M = V, Cr, Mn with X -p states, leading to a higher degree of covalence and reduced ionicity with increasing Zn-X bond length. Figure 4 displays the charge density plot for $ZnVX_2$.

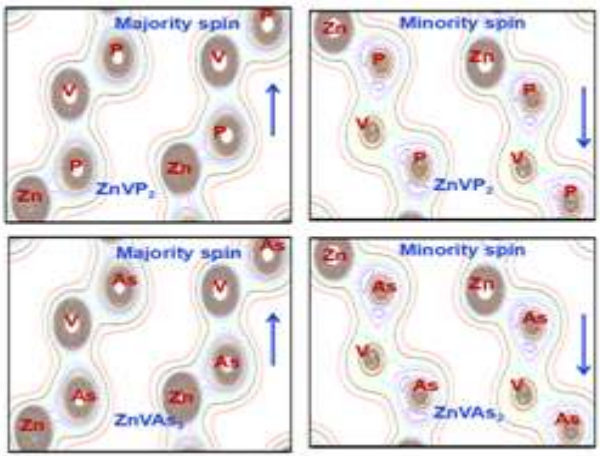

Figure 4: Valence Electron Charge Density Contour Plots in the (110) Plane for $ZnVX_2$ (X = P, As)

In the case of $ZnFeX_2$, the X anion moves closer to the Zn cation, resulting in a decrease in Zn-X bond length and stronger ionic character. Conversely, there is an increase in Fe-X bond length, reducing covalence due to the large electronegativity difference between Zn cations and X anions. Hence, the bonds in $ZnFeX_2$ are more ionic. These plots show valence electrons transferring from Zn and M atoms to X atoms.

Similarly, the charge density contour plots for all $CdMX_2$ compounds reveal charge transfer of valence electrons from Cd to X and M to X ions. Cd-X and Sc-X/Ti-X bonds exhibit a mixed ionic/covalent nature in $CdScX_2$ and $CdTiX_2$ compounds. In contrast, $CdMX_2$ (M = V, Cr, Mn) compounds display larger charge transfer between M and X ions, leading to M (V, Cr, Mn) cations moving closer to X (P/As) anions and a higher degree of covalence nature between X and M due to strong p-d exchange interaction. Figure 4.6 shows the charge density contours for $CdVX_2$, suggesting a high degree of covalence nature contributing to half-metallic ferromagnetism (HMF) in $CdMX_2$ compounds.

However, in $CdFeX_2$, X atoms move more toward Cd than Fe due to the significant electronegativity difference between X and Fe, resulting in stronger ionic character for Cd-X bond. This decrease in covalence or increase in ionic nature may lead to the absence of HMF.

Our results show that the charge density contour plots demonstrate a mixture of ionic and covalent characters for Cd-X and M-X atomic bonds in both spin channels for all compounds. The electronic charge distribution around X atoms indicates a significant accumulation of charge, leading to the formation of Cd-X and M-X bonds.

4. **Magnetic Moment:** Table 3 presents the calculated total and partial magnetic moments for all $ZnMX_2$ (M = Sc, Ti, V, Cr, Mn, Fe; X = P, As) compounds within GGA and LSDA. The total magnetic moments are found to be zero for $ZnScX_2$ and $ZnTiX_2$, while $ZnMX_2$ (M = V, Cr, Mn; X = P, As) compounds exhibit integer magnetic moments of 1.00 μ_B/f.u., 2.00 μ_B/f.u., and 3.00 μ_B/f.u. respectively. The formation of integer magnetic

moments is a characteristic feature of half-metallic ferromagnetism (HMF). However, for $ZnFeP(As)_2$ compounds, the calculated magnetic moments are 2.43 μ_B/f.u. (2.71 μ_B/f.u.) within GGA and 2.19 μ_B/f.u. (2.76 μ_B/f.u.) within LSDA, indicating stable ferromagnetism and the absence of HMF in these compounds.

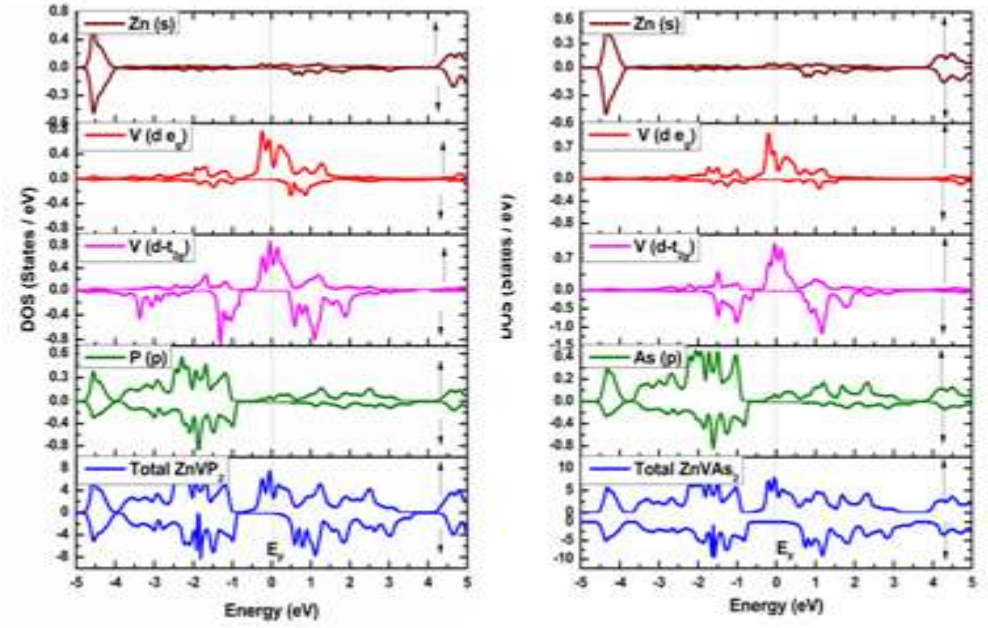

Figure 5: Spin-Dependent Total and Partial Density of States of $ZnVX_2$ (X = P, As)

The magnetic properties in all $ZnMX_2$ (Table 6) primarily arise from the contribution of M -3d like states. HMF is attributed to the hybridization of -3d t_{2g} states with the nearest neighbouring X (-p states) atoms, with a small contribution from Zn (-s states) atoms.

Moving on to $CdMX_2$, Table 7 lists the calculated total and individual magnetic moments. Non-spin polarization of energy states near the Fermi level results in zero magnetic moment at each atomic site of $CdScX_2$ and $CdTiX_2$ compounds. For $CdMX_2$ (M = V, Cr, Mn; X = P, As), the total magnetic moments are 1.00 μ_B/f.u., 2.00 μ_B/f.u., and 3.00 μ_B/f.u. respectively. However, in $CdFeP_2$ and $CdFeAs_2$, the calculated total magnetic moments are 1.83 μ_B/f.u. (1.64 μ_B/f.u.) and 1.94 μ_B/f.u. (1.84 μ_B/f.u.) per formula unit respectively under GGA (LSDA) approximations.

The absence of integer magnetic moments or HMF behavior in $CdFeX_2$ compounds can be attributed to the increase in the crystal field split energy of t_{2g} and e_g suborbital of -3d states in the Fe atom. This increased crystal field splitting energy reduces the space charge density of the Fe atom, leading to a broadening of valence bands and crossing of the Fermi level in the spin-down channel.

Table 6: Calculated Half-Metallic Gap (E_{HM}) in eV, Minority Spin Gap ($E_{g\downarrow}$) in eV, Partial, Interstitial and Total and Magnetic Moments in μ_B for $ZnMX_2$ (M = Sc, Ti, V, Cr, Mn, Fe; X = P, As) Compounds at their Equilibrium Volume using GGA and LSDA

Compounds	GGA							LSDA						
	E_{HM}	$E_{g\downarrow}$	Magnetic Moments					E_{HM}	$E_{g\downarrow}$	Magnetic Moments				
			Zn	M	Y	Int.	Total			Zn	M	Y	Int.	Total
$ZnScP_2$	-	-	0.04	0.09	0.2	0.89	0.843	-	-	0.05	0.12	0.16	0.64	0.82
$ZnTiP_2$	-	-	-	-	-	-	-	-	-	-	-	-	-	-
$ZnVP_2$	1.050	0.12	-	1.29	-0.08	0.25	**1.00**	1.04	0.14	0.01	0.89	-0.05	0.33	**1.00**
$ZnCrP_2$	0.954	0.28	0.01	2.08	-0.13	0.33	**2.00**	0.62	0.24	0.03	1.65	-0.05	0.60	**2.00**
$ZnMnP2_2$	0.643	0.53	0.02	1.05	-0.03	0.21	**3.00**	0.41	0.46	0.01	0.38	0.06	0.14	**3.00**
$ZnFeP_2$	-	-	0.03	1.61	-0.04	0.26	3.38	-	-	0.05	2.13	-0.04	0.28	3.37
$ZnScAs_2$	-	-	0.04	1.61	-0.04	0.26	2.43	-	-	0.61	0.93	0.53	0.86	2.19
$ZnTiAs_2$	-	-	-	-	-	-		-	-		-	-	-	-
$ZnVAs_2$	1.216	0.16	-	1.12	-0.10	-0.2	**1.00**	1.18	0.27	0.31	0.93	-0.05	0.32	**1.00**
$ZnCrAs_2$ **Present**	1.05	0.31	0.03	2.49	-0.18 -	-0.11 -	**2.00**	1.01	0.32	0.01	1.84	-0.07	0.53	**2.00**
Other[a]	1.01[a]	0.49[a]	-0.01[a]	2.33[a]	0.15 [a]	0.10 [a]	**2.00** [a]							
$ZnMnAs_2$	0.612	0.16	0.05	2.86	-0.06	-0.09	**3.00**	0.56	0.17	0.01	0.89	-0.02	0.17	**3.00**
$ZnFeAs_2$	-	-	0.03	2.11	-0.05	0.33	2.781	-	-	-0.0	2.09	-0.035	0.14	2.76

[a]Yu & Yao (2011)

Table 7: Calculated Half-Metallic Gap (E_{HM}) in eV, Minority Spin Gap ($E_{g\downarrow}$) in eV, Partial, Interstitial and Total and Magnetic Moments in μ_B for $CdMX_2$ (M = Sc, Ti, V, Cr, Mn, Fe; X = P, As) Compounds at their Equilibrium Volume Using GGA and LSDA

Compounds	GGA							LSDA						
	E_{HM}	$E_{g\downarrow}$	Magnetic Moments					E_{HM}	$E_{g\downarrow}$	Magnetic Moments				
			Cd	M	Y	Int.	Total			Cd	M	Y	Int.	Total
$CdScP_2$			-	-	-	-	-	-	-	-	-	-	-	-
$CdTiP_2$	-	-	-	-	-	-	-	-	-	-	-	-	-	-
$CdVP_2$	0.642	0.22	0.001	0.989	-0.069	0.294	**1.00**	0.459	0.55	0.001	0.689	-0.069	0.294	**1.00**
$CdCrP_2$	0.948	0.54	0.042	1.979	-0.132	0.655	**2.00**	0.405	0.42	0.032	1.479	-0.132	0.655	**2.00**
$CdMnP_2$	0.880	0.40	0.043	2.54	-0.13	0.46	**3.00**	0.525	0.75	0.033	2.14	-0.13	0.46	**3.00**
$CdFeP_2$			0.018	1.862	-0.022	0.26	2.49			0.010	1.462	-0.022	0.26	2.28
$CdScAs_2$	-	-	-	-	-	-	-	-	-	-	-	-	-	-
$CdTiAs_2$	-	-	-	-	-	-	-	-	-	-	-	-	-	-
$CdVAs_2$	0.856	0.24	-0.005	1.544	-0.043	0.085	**1.00**	0.288	0.78	-0.03	1.244	-0.033	0.075	**1.00**
$CdCrAs_2$	1.153	0.60	0.009	2.088	-0.056	0.153	**2.00**	0.424	0.93	0.006	1.888	-0.046	0.143	**2.00**
$CdMnAs_2$	0.884	0.16	0.040	3.545	-0.074	0.163	**3.00**	0.696	0.86	0.020	3.145	-0.064	0.123	**3.00**
$CdFeAs_2$			0.003	1.932	-0.031	0.079	2.83			0.001	1.932	-0.021	0.069	2.63

IV. CONCLUSION

In conclusion, this research focuses on the search for new magnetic materials suitable for spintronic applications. Specifically, II-IV-V_2 ($ZnMX_2$ and $CdMX_2$; M = Sc, Ti, V, Cr, Mn, Fe; X = P, As) chalcopyrite's are investigated by substituting M atoms at the site of group IV (Ge) atoms in $ZnGeX_2$ and $CdGeX_2$ (X = P, As) compounds. Theoretical calculations using the self-consistent FP-LAPW method with LSDA and GGA exchange-correlation effects within the DFT framework were employed for a detailed analysis of the structural phase stability, ground-state, electronic, and magnetic properties.

The II-IV-V_2 compounds were found to exist in ordered body-cantered tetragonal (BCT) chalcopyrite, disordered zinc-blende (ZB), and cubic $L2_1$ structures. Total energy vs. volume calculations indicated the BCT chalcopyrite structure to be the most stable. Further calculations were performed for $ZnMX_2$ and $CdMX_2$ compounds in the BCT chalcopyrite structure using non-spin-polarized and spin-polarized (FM and AFM) methods.

Key observations and conclusions from the investigation include the stability of all $ZnMX_2$ compounds in the BCT chalcopyrite structure, with FM stability observed for $ZnMX_2$ (M = V, Cr, Mn, Fe) except $ZnScX_2$ and $ZnTiX_2$. Spin-polarized electronic band structure calculations revealed half-metallic FM properties for $ZnMX_2$ (M = V, Cr, Mn; X = P, As) compounds with specific magnetic moments per formula unit. $ZnFeX_2$ compounds showed stable FM properties as well. The formation energy of these compounds confirmed their stability under experimental synthesis conditions.

Regarding $CdMX_2$ (M = Sc, Ti, V, Cr, Mn, Fe; X = P, As) compounds, most of them displayed FM stability, except for $CdScX_2$ and $CdTiX_2$ which remained non-magnetic at equilibrium. The calculated lattice constants for the studied compounds were comparable to other chalcopyrite's and zinc-blende-based semiconductors. Experimental studies using X-ray photoelectron spectroscopy or photoemission techniques are suggested to determine the electronic band structure of these compounds. Additionally, future work may involve calculations for defect formation energy, exchange-coupling constant, and Curie temperature to further guide experimental synthesis efforts. Overall, this study provides valuable insights into the properties of chalcopyrite compounds, contributing to the exploration of new magnetic materials for spintronic applications.

REFERENCES

[1] J. Hafner, C. Wolverton, and G. Ceder, "Toward Computational Materials Design: The Impact of Density Functional Theory on Materials Research," Mater. Res. Soc. Bull. 31, 659–668 (2006).
[2] S. A. Wolf et al., "Spintronics: A Spin-Based Electronics Vision for The Future," Science 294, 1488 (2001).
[3] J. Rufinus, "Magnetic Properties of M-doped (M = Mn, Cr, or V) ZnSiN2," J. Appl. Phys. 105, 07C509 (2009).
[4] J. B. Goodenough, "Metallic Oxides," Prog. Solid State Chem. 5, 145–399 (1971).
[5] C. Hofner et al., "Stoichiometry-, Phase- and Orientation-Controlled Growth of Polycrystalline Pyrite (FeS2) Thin Films By MOCVD," J. Cryst. Growth 151, 325–333 (1995).
[6] G. Jaiganesh and G. Kalpana, "First-principles study of structural, electronic and magnetic properties of AeX (Ae = Be, Mg, Sr, Ba; X = Si, Ge, and Sn) compounds." Journal of magmetism and magnetic materials, 326, 66-74 (2013).

[7] G.Jaiganesh, R.D. Ethiraj, G.Kalpana and M.Rajagopalan, "Ab-initio band structure calculations of half-metallic calcium pnictides, Physica Status Solidi (b), 244(12),4643-4650,(2007)
[8] L. H. Thomas, "The Calculation of Atomic Fields," Math. Proc. Camb. Phil. Soc. 23, 542–548 (1927).
[9] G. A. Medvedkin et al., "Room Temperature Ferromagnetism In Novel Diluted Magnetic Semiconductor Cd1-xMnxGeP2," Jpn. J. Appl. Phys. Part 2 39, L949 (2000).
[10] G. A. Medvedkin et al., "New Magnetic Materials in ZnGeP2-Mn Chalcopyrite System," J. Cryst. Growth 236, 609–612 (2002).
[11] S. Picozzi, Y. Zhao, and A. J. Freeman, "Mn-doped CuGaS2 chalcopyrites: An Ab Initio Study Of Ferromagnetic Semiconductors," Phys. Rev. B 66, 205206 (2002).
[12] L. H. Yu and K. L. Yao, "Half-Metallic Ferromagnetism of Chalcopyrite ZnCrAs2: A First-Principles Prediction," J. Appl. Phys. 109, 016111–016113 (2011).
[13] H. Nakamura et al., "Tunable Photoluminescence Wavelength of Chalcopyrite CuInS2-Based Semiconductor Nanocrystals Synthesized in a Colloidal System," Chem. Mater. 18, 3330–3335 (2006).
[14] B. Djebour et al., "Structural, Magnetic and Optoelectronic Properties of CuMnSe2-Chalcopyrite: DFT+U and Hybrid Functional Investigation," J. Supercond. Novel Magn. 31, 1881–1893 (2018).
[15] Kohn, W & Sham, L.J 1965, 'Self-Consistent Equations Including Exchange and Correlation Effects', Physical Review, vol. 140, no. 4A, pp. A1133-A1138.
[16] P. Blaha et al., "WIEN2K-An Augmented Plane Wave and Local Orbital Program for Calculating Crystal Properties," Technische Universitat Wien, Austria, 2001.
[17] Perdew, J.P, Burke, S & Ernzerhof, M 1997, 'Generalized Gradient Approximation Made Simple', Physical Reviews letters, vol, 78, pp. 3865-3868.
[18] Perdew, J.P & Wang, Y 1992, 'Accurate and Simple Analytic Representation of The Electron-Gas Correlation Energy', Physical Reviews B, vol. 45, pp. 13244.
[19] F. Birch, "Finite Elastic Strain of Cubic Crystals," Phys. Rev. 71, 809 (1947).
[20] L. H. Yu, "Half-Metallicity and Strong Exchange Interactions of CuCrSe2 in Chalcopyrite Structure: A First-Principles Calculation," Comput. Mater. Sci. 65, 287–290 (2012).
[21] Y. J. Zhao and A. Zunger, "Zinc-Blende Half-Metallic Ferromagnets are Rarely Stabilized by Coherent Epitaxy," Phys. Rev. B 71, 132403 (2005).
[22] A. Janotti et al., "Structural and Electronic Properties of ZnGeAs2," Phys. Rev. B 63, 195210–195217 (2001).
[23] J. L. Shay and J. H. Wernick, "Ternary Chalcopyrite Semiconductors: Growth, Electronic Properties and Applications," Pergamon Press, Oxford, 1975.
[24] A. J. Spring-Thorpe and B. R. Pamplin, "Growth of Some Single Crystal II-IV-V2 Semiconducting Compounds," J. Cryst. Growth 3, 313–316 (1968).
[25] H. L. Skriver, "The LMTO Method. Muffin-tin Orbitals and Electronic Structure," Springer, Heidelberg, 1984.
[26] Y. J. Zhao et al., "Comparison of Predicted Ferromagnetic Tendencies of Mn Substituting the Ga Site in III–V's and in I–III–VI2 Chalcopyrite Semiconductors," Appl. Phys. Lett. 84, 3753 (2004).
[27] C. Shiyou and X. G. Gong, "Band-Structure Anomalies of the Chalcopyrite Semiconductors CuGaX2 Versus AgGaX2 (X=S and Se) and their alloys," Phys. Rev. B 75, 205209 (2007).
[28] N. H. Hong et al., "Ferromagnetism in Transition-Metal-Doped TiO2 Thin Films," Phys. Rev. B 70, 195204 (2004).
[29] O. K. Andersen and R. V. Kasowski, "Electronic States as Linear Combinations of Muffin-Tin Orbitals," Phys. Rev. B 4, 1064–1069 (1971).

